Final Report

Project Title

CRC 2023 P0070

Nano-Modified Calcined Clay-Based Cement Concrete: A High Modulus Concrete with Low Carbon Footprint

Prepared for the ACI Foundation

Principal Investigator

Panagiotis A. Danoglidis
Assistant Professor
The University of Texas at Arlington

Project start date: 25 August 2023

(a) Acknowledgement of support

The PI and the research team would like to acknowledge the financial support of ACI Foundation and its Concrete Research Council (CRC) for the research grant # CRC 2023 P0070 "Nano-Modified Calcined Clay-Based Cement Concrete: A High Modulus Concrete with Low Carbon Footprint". Master Builders Solutions Admixtures US, LLC is kindly acknowledged for supplying metakaolin.

The advisory committee is gratefully acknowledged for overseeing and evaluating the research progress of this project.

Primary Champion

Kamal Khayat
Vice Chancellor for Research and Innovation
Vernon and Maralee Jones Endowed Professor of Civil Engineering
Missouri University of Science and Technology
Voting Member of ACI TC 236

Industrial Liaison

Frank Ong
Senior Scientist
Master Builders Solutions U.S. LLC

(b) Declaration of Competing Interest

The PI and research team of the project declare that they have no known competing financial interest or personal relationships that could have appeared to influence the work reported in this project.

Table of Contents

Executive Summary

The aim of this research project is to design resilient concrete by replacing high volumes of ordinary Portland cement (OPC) with calcined clay and reinforcing the cementitious matrix with carbon-based nanomaterials. Replacing OPC at volumes greater than 10% with calcined clay materials, such as metakaolin (MK), is a promising strategy for enhancing concrete's compressive strength due to its densified microstructure. However, MK-based cement concrete exhibits brittle behavior and low tensile properties.

An effective approach to address this limitation is to incorporate 1D carbon nanotubes (CNTs) and carbon nanofibers (CNFs), which have been shown to significantly improve the tensile strain capacity of engineered concrete. The key objective of the research is to precisely control and optimize the nanoscale chemical and mechanical properties of the sub-10 nm interfaces between cement hydration products, MK, and nanomaterials; and the nanomodified cement/aggregate Interfacial Transition Zone (ITZ) for the successful design of concrete with optimum bulk mechanical performance.

The experimental study demonstrates that the addition of small amounts of well-dispersed CNTs (0.1 wt% by mass of binder) in MK-based cementitious composites can lead to substantial improvements in the modulus of elasticity (MOE) and post-crack ductility. The pozzolanic reaction of MK densifies the microstructure, resulting in a 21% improvement in compressive strength and a 34% increase in MOE compared to OPC mortar. Compared to MK-OPC mortar, the CNT-reinforced MK-OPC mortar nanocomposite exhibits an 88% increase in flexural strength and a 107% increase in MOE. Additionally, the tensile strain energy absorption capacity improved by 1.8 times at the elastic stage. The I_5, I_{10}, and I_{20} toughness indices showed improvements ranging from 45% to 110%, demonstrating the ability of the MK-based cementitious nanocomposite to absorb energy at the post-crack stage. These improvements are attributed to the reinforcing efficiency of multi-walled carbon nanotubes (MWCNTs), which enhance the ultimate strain capacity and prolong both the elastic stage and failure onset in nanoreinforced mortars.

Impact Statement

The research plan of this project lays the foundation for the detailed optimization of cutting-edge concrete formulations for next-generation resilient structural materials. This scientific direction, including testing and validation across different scales, significantly contributes to the development of a comprehensive nano-to-macro scale research framework. This framework will support the tailoring and tuning of complex cementitious matrix properties for targeted applications, such as the design of high-modulus concrete for tall buildings.

1. Introduction

The concrete industry currently accounts for 6%-8% of the global CO_2 emissions, and cement manufacturing is projected to keep increasing to match the growing urbanization needs. One of the most common ways of reducing the carbon footprint of the cement and concrete industry, in line with the Paris Agreement on climate change, is by replacing a part of Ordinary Portland Cement (OPC) with a supplementary cementitious material (SCM). Traditional SCMs, such as fly ash and slag cement, are limited in quantity, and their availability is tied to the production capacity of their respective industries [1,2]. Metakaolin (MK) is a highly reactive alumino-silicate and is formed by the dihydroxylation of kaolinitic clay in a temperature range of 700-800 °C [3,4]. The calcination of clay produces 70% lower CO_2 emissions than OPC [5]. The addition of MK in cement, when properly dispersed, can densify the microstructure and considerable improvements in compressive strength are observed [6]. Shekarchi et al. [7] observed an increase of 20% in compressive strength on replacing 15% cement with metakaolin. Partial replacement of cement with a fine sized pozzolan such as metakaolin has been found to densify the interfacial transition zone (ITZ) because of the micro-filler effect [8–10]. However, concrete made with MK exhibits limited tensile strain capacity due to its brittle nature.

On the other hand, addition of small amounts of highly dispersed carbon nanotubes (CNTs) to cement based matrices, up to 0.1 wt% of cement, can significantly improve the modulus of elasticity, by 100%, flexural strength, by 85%, and fracture properties, by 120% [11–14]. It is envisioned that combining MK with carbon-based nanomaterials may lead to distinct changes of the cementitious matrix at the nanoscale and improve the overall mechanical performance and durability.

The key objective of the research is to enhance the energy absorption capability and tensile load carrying capacity of metakaolin based cementitious composites by successfully incorporating highly dispersed CNTs. The flexural strength and modulus of elasticity is evaluated using the three-point bending tests on notched beam specimens. The effect of CNTs on the elastic and post-elastic stages of the composite is assessed by evaluating the first-crack toughness and size independent toughness indices through a detailed study of the load-crack mouth opening displacement (CMOD) response of the notched specimens.

1st Reporting Period: The results of the experimental study conducted during the 1st reporting period of the project showed that the addition of small amounts of well-dispersed CNTs, 0.1 wt%, by mass of binder, in metakaolin-based cementitious mortars with 20% replacement can lead to substantial improvements in MOE and post-crack ductility. The pozzolanic reaction of MK densifies the microstructure leading to an improvement in compressive strength by 21% and MOE by 34% compared to OPC mortar. Compared to the MK-Mortar, the CNT reinforced MK-Mortar nanocomposite exhibited 88% increase in flexural strength and 107% increase in MOE. Moreover, the tensile strain energy absorption capacity was improved by 1.8x at the elastic stage. The I_5, I_{10} and I_{20} toughness indices showed improvements of 45%-110%, which demonstrates the ability of the MK-based mortar nanocomposite to absorb energy at the post-crack stage. This performance can be related to the proper function of MWCNTs in bridging nano cracks, prolonging the elastic stage and increasing the ultimate strain capacity of nanoreinforced mortars.

2nd Reporting Period: The objective of the research activities for the 2nd reporting period of this project is the study and characterization of the chemical and mechanical properties at the interfacial transition zone (ITZ) between the fine aggregate (sand) and CNT reinforced cementitious matrix. The results will be used as input data for the research activities of the final reporting period targeting the design and development of nanoengineered concrete mixes with optimum mechanical and fracture properties by maximizing the amount of replacement of OPC with MK and reinforcing the matrix with CNTs.

3rd Reporting Period: Concrete mixes integrated with MK-CNT blend were designed and tested to evaluate mechanical and fracture properties. Based on the observations from the previous reporting period, additional nanoscale mechanical properties were determined at the ITZ between aggregate and CNT reinforced cementitious matrix. These properties, namely modulus of elasticity and elastic strain energy dissipation of the ITZ were assessed to understand the macro-mechanical fracture response of the notched beam CNT reinforced MK-concrete specimen.

2. Materials and Specimens

Mixtures were produced using Type-I Ordinary Portland Cement (OPC) and standard Ottawa sand according to ASTM C778-17. Metakaolin with the commercial name Masterlife MK 828 conforming to the ASTM C618 was used as OPC replacement at an amount of 20 wt%. Multi-walled carbon nanotubes were used at an amount of 0.1 wt% of cementitious binders. The geometrical and physical properties of CNTs are shown in the Table 1.

An ultrasonication procedure was adopted to homogenously disperse the CNT in the mixing water. The CNTs were added to the aqueous solution containing polycarboxylate-based surfactant. The weight ratio of surfactant to CNTs was kept fixed at 4 to achieve effective dispersion. Ultrasonication energy was supplied from a 500 W cup-horn high intensity ultrasonic processor with a 19-mm diameter probe. The amplitude of the sonicator was kept at 57% to deliver a constant energy of 1900-2100 J/min. The procedure was performed at room temperature, and in order to avoid overheating, the operation cycle was limited to 20 s. Figures 1 (a) and (b) show the "As received" CNTs before the ultrasonication process and individual CNTs after sonication in surfactant aqueous suspension, respectively.

***Table 1**: Properties of multiwalled carbon nanotubes (CNTs)*

Diameter, nm	20-45
Length, µm	≥ 10
Purity, %	> 98
Surface area, m^2/g	> 200
Aspect ratio	307

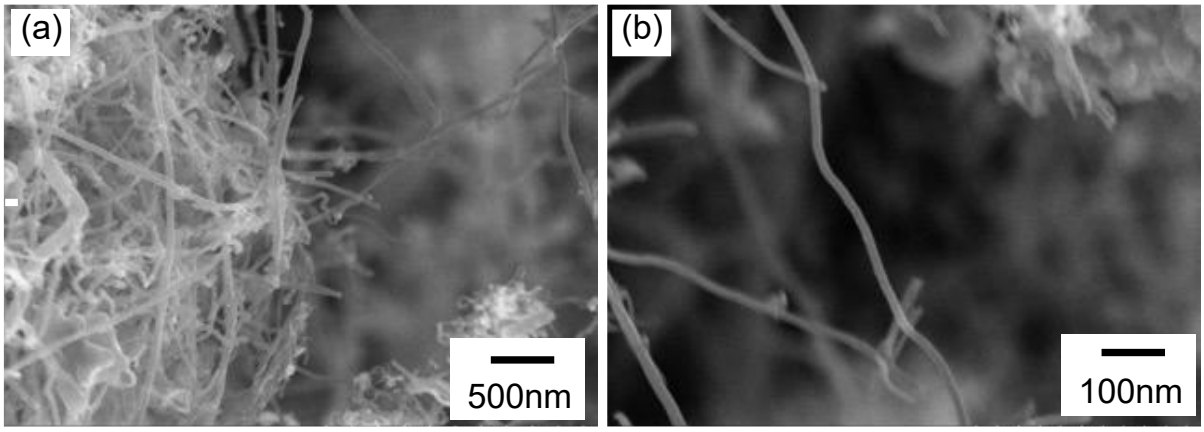

***Figure 1**: SEM images of (a) "As received" CNTs and (b) Individual CNT in surfactant aqueous suspension*

The chemical composition of OPC and MK is listed in Table 2. SEM image of Metakaolin (Figure 2) shows a fine sized platelet shaped structure. Characterization of MK was performed using XRD (Figure 3) and was found to be highly amorphous with a quartz peak at 25° (2θ) [15].

***Table 2**: Chemical composition (% by weight)*

Oxides	OPC	MK
SiO_2	19.50	55
Al_2O_3	3.52	40
Fe_2O_3	3.37	1.4
CaO	66.90	0.30
K_2O	0.60	0.4
TiO_2	0.21	1.50
Na_2O	0.92	0.40

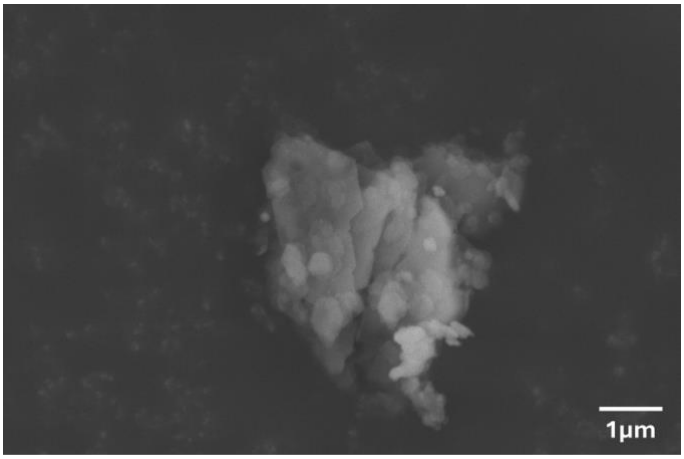

***Figure 2**: SEM image of Metakaolin*

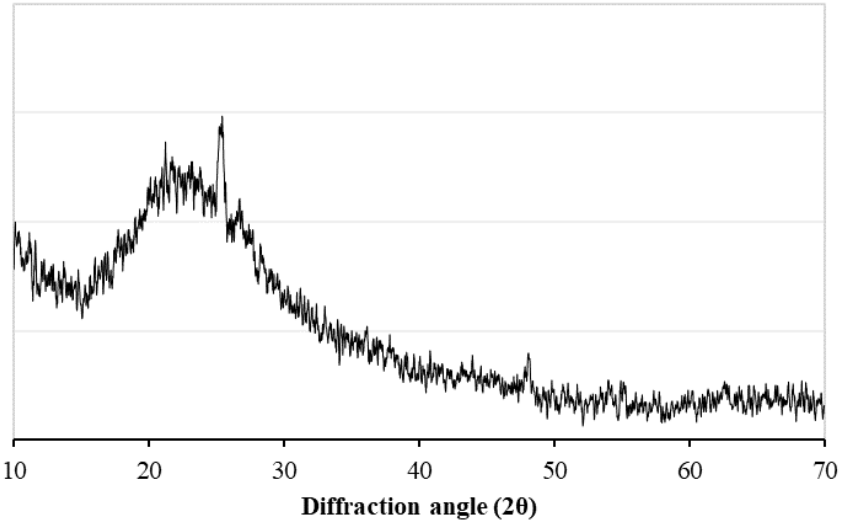

***Figure 3**: XRD characterization of MK*

The mixing of mortar specimens was conforming to ASTM C305. The water to binder ratio (w/b) and sand to binder ratio (s/b) was kept at 0.40 and 2.75, respectively. After mixing, cement mortars were cast in prismatic molds of 4×4×16 cm. After demolding, samples were kept in the curing chamber at a temperature of 23 ºC and 95% humidity until the time of testing.

Conventional concrete was produced at a w/c ratio of 0.51. The amount of cement was kept at 380 kg/m^3. Dry siliceous natural sand, calibrated to 0/4.75 mm conforming to standard ASTM C33/C33M-24a, and graded crushed limestone up to a nominal size of 16 mm, were used as fine and coarse aggregates. The mix design is shown in Table 3. The mixing procedure adopted was in accordance with ASTM C192/C192M-24. Concrete was cast in 7×8×38 cm oiled prismatic molds for the three-point bending tests and another set-in cylindrical molds at a height of 14 cm and a diameter of 7 cm for the uniaxial compression experiments. All specimens remained molded for 24 h and were stored in the curing room (23 ºC, 95% humidity) after demolding.

***Table 3**: Mix design of concrete specimens (by parts)*

Specimen	CNTs	Water	Cement	MK	Sand	Coarse aggregates
M	-	0.51	1.0	-	2.63	2.04
M+CNT	0.1	0.51	1.0	-	2.63	2.04
M+MK	-	0.51	0.8	0.2	2.63	2.04
M+CNT+MK	0.1	0.51	0.8	0.2	2.63	2.04

3. Experimental Methods

3.1. *Determination of Macro-Mechanical Properties*

Three-point bending test was carried out on notched beam specimens using Linear Elastic Fracture Mechanics (LEFM). A notch of 13 mm length was introduced into the prismatic 4×4×16 cm specimens using a water cooled saw machine. The length of the notch was chosen to keep the notch to depth ratio around 1/3. The test was performed using a 30 kN MTS servo-hydraulic, closed-loop testing machine under displacement control. An extensometer is

attached to the notch to record the crack mouth opening displacement (CMOD). The compressive strength was determined using the two halves of the prism, resulting from the fracture of the three-point bending specimen. The flexural strength, σ_f is calculated by using the equation:

$$\sigma_f = \frac{3FL}{2b(t-a_0)^2} \qquad \textit{eq. 1}$$

Where L, b, t and a_0 are the length, thickness, breadth and notch depth, respectively of the specimen as presented in Figure 4.

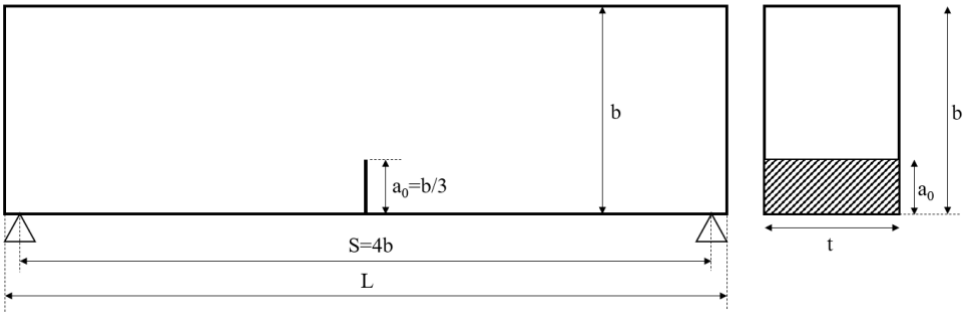

***Figure 4**: Experimental setup of Linear Elastic Fracture Mechanics test*

The Young's modulus ($\boldsymbol{E}$) is calculated using the fracture model proposed by Jenq and Shah [16] given by the following equation:

$$E = \frac{6Sa_0 g_2(a_0)}{C_i b^2 t} \qquad \textit{eq. 2}$$

Where S, b, t and a_0 are length between supports, thickness, breadth and notch depth of the specimen, respectively as shown in the Figure 2. $\boldsymbol{C_i}$ (mm/N) is the initial compliance and can be calculated with the load-CMOD curve. The geometric function, $g_2(a_0)$ is given by:

$$g_2(a_0) = 0.76 - 2.28a_0 + 3.87a_0^2 - 2.04a_0^3 + \frac{0.66}{(1-a_0)^2} \qquad \textit{eq. 3}$$

Flexural toughness was calculated by taking the area under the load-CMOD curve. The post-crack part of the load-CMOD curve is analyzed using the toughness indices which are calculated as per the ASTM C1018-97 using the equation:

$$Toughness\ indice\ (I) = \frac{Area\ under\ load-deflection\ curve\ upto\ a\ specified\ deflection\ criterion}{Area\ upto\ deflection\ at\ which\ first\ crack\ is\ deemed\ to\ have\ occured} \qquad \textit{eq. 4}$$

Compression strength was determined after flexural testing on samples corresponding to the two halves of the prism, as per ASTM C349-18. A 500 kN MTS servo-hydraulic closed-loop testing machine operating at a loading rate of 0.05 mm/s was used for the compressive strength testing. In accordance with ASTM C348-21 and ASTM C349-18, specimens with spread in strength (both flexural and compression strengths) greater than 10% from average values of all test specimens made from the same batch and tested at the same period were not considered.

Three-point bending test was performed on the 28d concrete beams following the ASTM C293/C293M-16 to determine the flexural strength and Young's modulus. The test was performed using the aforementioned 30 kN MTS servo-hydraulic, closed-loop testing machine under displacement control. The rate of displacement was kept at 0.1 mm/min. Uniaxial compression experiments were also conducted on cylindrical concrete specimens to investigate the compressive strength according to the ASTM C39/C39M-18. The test was performed using a 250 kN MTS servo-hydraulic, closed-loop testing machine under displacement control. The rate of displacement was kept at 0.3 mm/s.

3.2. *Scanning Electron Microscopy (SEM) Imaging*

The microstructure of the samples was examined using a Hitachi SEM (Figure 5), operating in high vacuum mode with a 10 mm working distance. An acceleration voltage of 15 kV was maintained for Backscattered mode (BSE) and Energy Dispersive X-Ray Analysis (EDX) data acquisition. The specimens were prepared and polished using diamond suspensions (3 µm, 1 µm, 0.5 µm, 0.25 µm and 0.1 µm) on a polishing cloth. To remove any residual polishing debris, the sample surface was cleaned with a Hitachi IM 4000 ion milling machine. A gold-palladium alloy was applied to the surface using a sputtering machine to avoid charging effects.

Figure 5*: Scanning Electron Microscope and Energy Dispersion X-ray Spectroscopy (SEM-EDX) at the CACM lab, University of Texas at Arlington*

3.3. *AFM Sample Preparation*

The polishing of mortar specimens was carried out with silicon carbide papers of different grit sizes 120, 240, 400, 600, 800 and 1200 for one minute each. Following this, the specimens were polished with diamond suspension (3 µm, 1 µm, 0.5 µm, 0.25 µm and 0.1 µm) and a 50 nm-gradation aluminium suspension on a plain polishing cloth. To remove any polishing debris, the sample surface was cleaned using a Hitachi IM 4000 ion-milling machine.

3.4. *AFM Test Parameters*

PeakForce QNM is a contact-based measurement method wherein the tip directly interacts with the sample, potentially causing surface scratches if the surface is not sufficiently smooth. Thus, a smooth surface is crucial for obtaining precise information and mechanical properties of the test area. To verify the thoroughness of the polishing, the spectral Root-Mean-Square (RMS) amplitude is assessed within the ITZ on a 50×50 μm^2 area. As observed in Table 4, the roughness RMS values for the test samples were less than 100 nm, which are deemed acceptable for conducting an AFM-QNM test.

Table 4: *RMS roughness over 50×50 µm² area*

Sample	Roughness (nm)
OPC	62.1
OPC+MK	68.0
OPC+CNT	80.6
OPC+CNT+MK	74.9

A tip of spring constant 200 N/m is employed for the AFM measurements. Prior to measurement, calibration is necessary for deflection sensitivity and tip radius. Deflection sensitivity is calibrated using a clean sapphire sample, while the tip radius is calibrated using a highly oriented pyrolytic graphite (HOPG) sample, which exhibits a modulus of elasticity similar to that of cement sample. Following calibration, the deflection sensitivity and tip radius are entered as calculation parameters in the AFM software. Once the calibration procedure is completed, the sample is placed in the AFM under the tip as shown in Figure 6. The tip is then brought close to the aggregate boundary within the interfacial transition zone. A 10×10 µm² area is selected in the ITZ where the tip is engaged to the sample surface.

(a) (b)

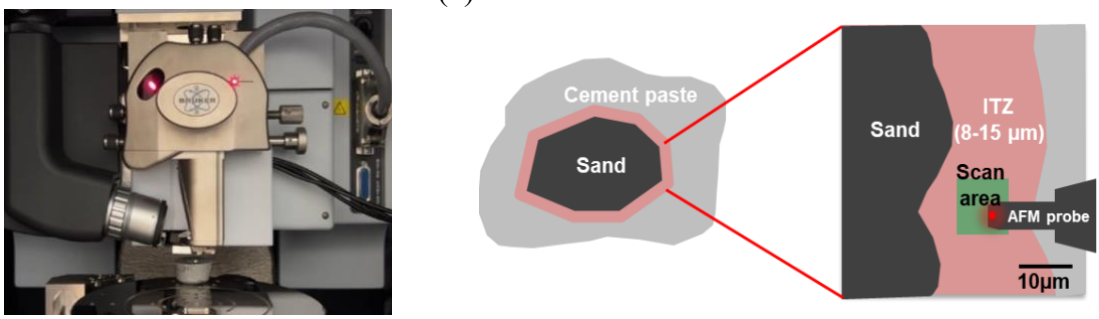

Figure 6: (a) *Nano-IR Atomic Force Microscopy at the CACM Lab, University of Texas at Arlington* ***(b)*** *Schematic representation of the test method*

Subsequently, the probe indents a designated area of interest on the sample at a scanning rate of 0.5 Hz and a resolution of 256 by 256 pixels within the ITZ as shown in Figure 6. The tip approaches the specimen surface where it experiences the attractive forces (van Der Waals forces) causing it to descend and make contact with the specimen surface (Figure 7). The tip continues to exert the force until it reaches the setpoint force of 100 nN. The value of force is chosen to stay within the elastic region of the loading curve. After the setpoint force is reached, the tip begins to ascend, and reverts to its initial position after overcoming the adhesion force. The linear region of the force-deflection curve of the unloading cycle is used to determine the Modulus of the specimen [17]. A Poisson ratio value of 0.3 is assumed for the calculations.

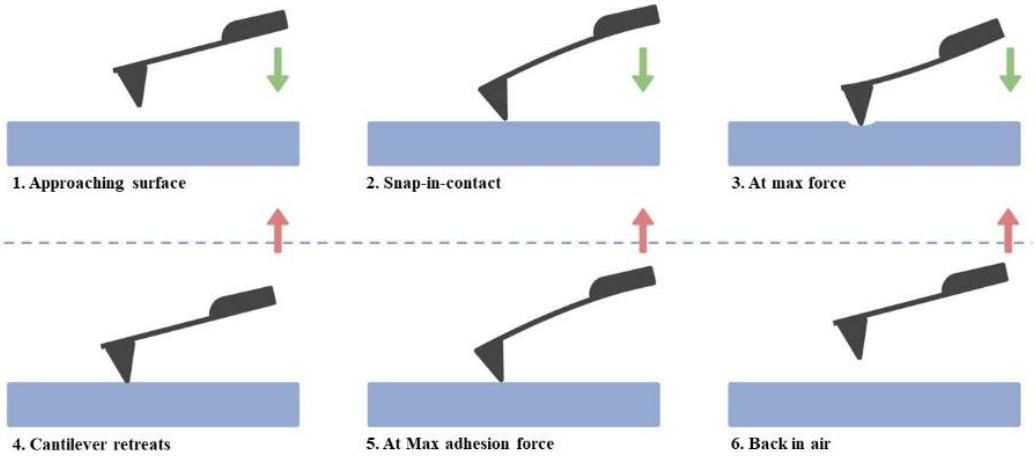

Figure 7: *Schematic representation of the experimental procedure involved in QNM*

4. Results and Discussions

4.1. *Flexural Strength, Modulus of Elasticity and Energy Absorption Capability of Mortar Specimens*

The flexural strength results at 3, 7 and 28 days for notched beam mortar samples made with 0.1 wt% CNT (Mortar+CNT), MK at 20% replacement (MK-Mortar) and 0.1 wt% and 20% MK (MK-Mortar+CNT) are shown in Figure 8. The replacement of cement with 20% MK into plain mortar resulted in 25% increase in flexural strength at 28 days. The incorporation of 0.1 wt% CNTs to the MK mortar exhibited an increase in flexural strength by 88% and 77% compared to plain mortar and MK-Mortar, respectively. The enhanced load bearing capacity of the CNT reinforced mortar and MK-mortar can be attributed to the high surface area and aspect ratio of CNTs (Table 1) and their homogeneous distribution within the cementitious matrix, which can induce strong interactions with the cementitious products, resulting in crack inhibition of the mortar and MK-mortar matrices.

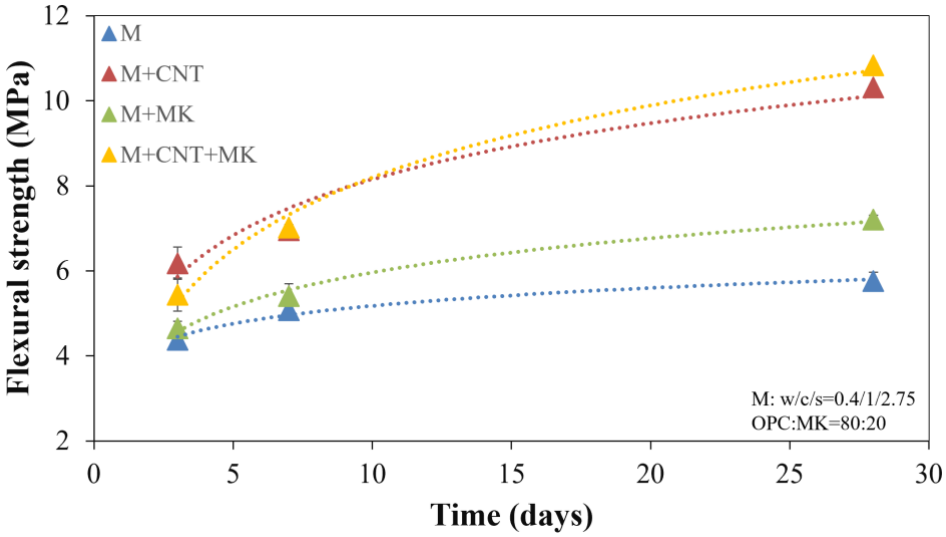

Figure 8*: Evolution of flexural strength with curing time of plain mortar and mortars made with 0.1 wt% CNT, 20% MK and both 0.1 wt% CNT and 20% MK*

Figure 9 illustrates the MOE results for the mortars containing CNT, MK and CNT+MK. The development of MOE over hydration time follows a similar trend to the flexural strength. Replacing 20% cement with MK resulted in a 34% increase in MOE compared to plain mortar, while the addition of 0.1 wt% CNT increased the MOE by 85%. The combination of 0.1 wt% CNTs and 20% MK showed improvements in MOE by, 107% and 73%, over the plain mortar and MK-mortar at 28 days, respectively.

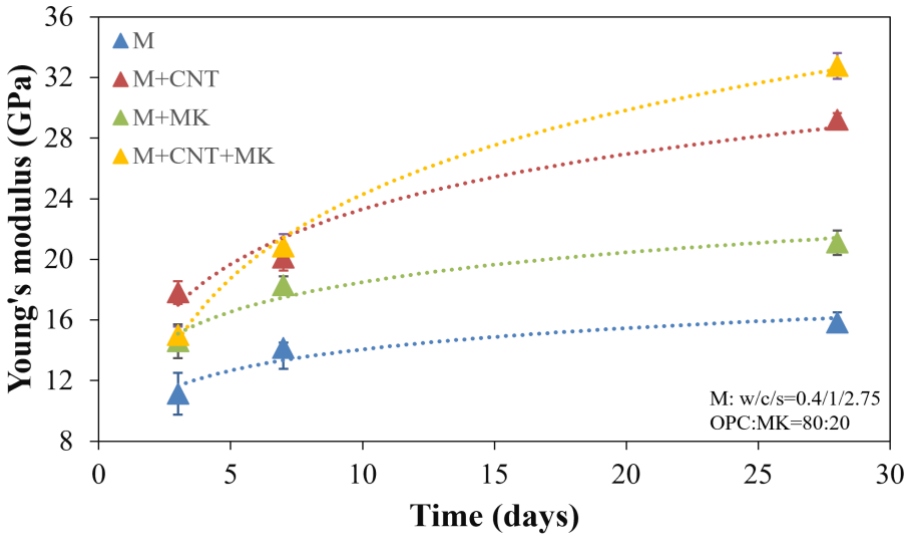

Figure 9: *Young's modulus of plain mortar and mortars with 0.1wt% CNT, 20%MK and both 0.1wt% CNT and 20% MK at 3, 7 and 28 days*

The flexural toughness is calculated by assessing the area under the load-CMOD curve of 28-day specimens (Figure 10), as outlined in Table 4. It represents the energy required for the material failure. LEFM tests on notched beam specimens reduces the variability of the crack path, non-symmetry of the deformation and hence reduces the errors involved in the determination of toughness calculation [18]. The incorporation of 20% MK to plain mortar led to moderate improvement of 40% in flexural toughness. A substantial improvement of 99% over plain mortar was observed for nano-reinforced mortar. The addition of CNT to the MK mortar exhibited a significant improvement of 130% in flexural toughness compared to the plain mortar, hence a considerable increased in energy requirement for crack propagation.

As per the ASTM C1018-97, the point on the initial portion of the load-CMOD curve after which the slope of the curve exhibits a definite change is identified, and the deflection value corresponding to that point is termed as the first crack length (δ). The toughness indices I_5, I_{10} and I_{20} (Table 5) are obtained as per ASTM C1018-97 by taking the ratios of the area in the load-CMOD curve up to deflection values of 3, 5.5 and 10.5 times of the δ value, respectively, to the area under the curve up to first crack. The first crack also marks the onset of cracking in the specimen. The toughness indices reflect the material's ability to carry loads post the initial crack formation and absorb energy after first cracking. Higher toughness indices also signify a better ability of the specimen to transfer tensile stresses across cracks which is a crucial performance factor for serviceability. Both the M+CNT+MK and M+CNT mixtures exhibited remarkable post-cracking load-bearing capacity, with increase in flexural toughness by 110% and 98%, respectively.

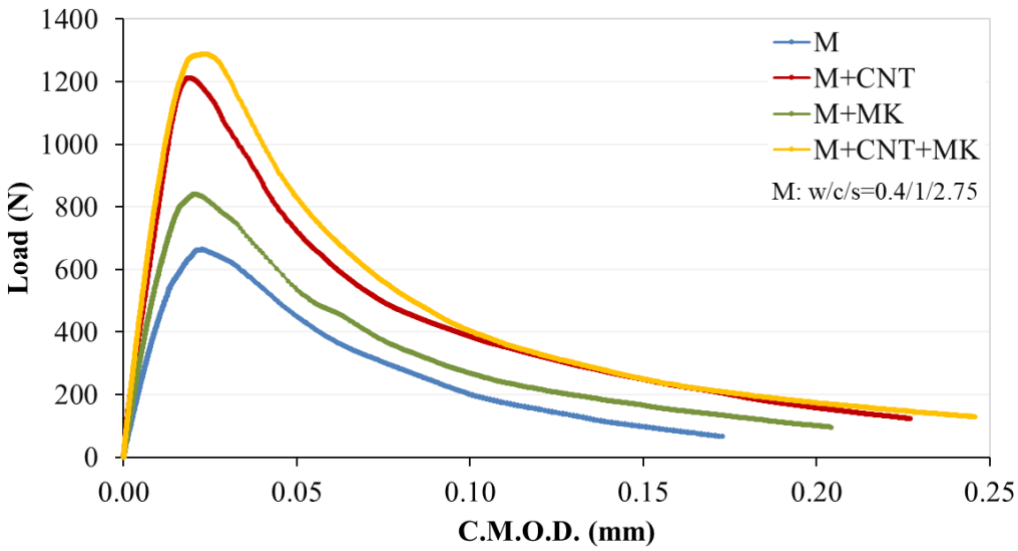

Figure 10: *Load-CMOD curve of plain mortar and mortars with 0.1wt% CNT, 20%MK and both 0.1wt% CNT and 20% MK at 28 days*

Table 5*: Toughness indices (I_5, I_{10} and I_{20}) and flexural toughness of 28 day specimens*

Specimen	Flexural Toughness (N-mm)	I_5	I_{10}	I_{20}
M	49.42	4.3 ± 0.08	7.2 ± 0.27	9.6 ± 0.28
M+CNT	98.55	5.1 ± 0.15	8.3 ± 0.60	11.7 ± 0.61
M+MK	69.42	4.6 ± 0.07	7.6 ± 0.10	10.8 ± 0.12
M+CNT+MK	113.47	6.7 ± 0.42	9.5 ± 0.27	12.6 ± 0.59

4.2. ***Compressive Strength***

Table 6 presents the compressive strength values obtained at 3, 7 and 28 days. The substitution of OPC by 20% MK resulted in 21% increase in compressive strength. An improvement of 23% in compressive strength was observed from 7 to 28 days of hydration for the metakaolin mortar (M+MK). This can be attributed to the fact that the pozzolanic reaction of MK reached peak values between 7 and 14 days [19]. The inclusion of CNTs led to a marginal increase in compressive strength, which aligns with findings from previous research by Danoglidis et al [14]. Specifically, the incorporation of CNTs in the mortar and MK-Mortar matrices resulted in low improvements in compressive strength of 11% and 2%, respectively.

Table 6*: Compressive strength of plain mortar and mortars with 0.1 wt% CNT, 20% MK and both 0.1% CNT and 20% MK at 3, 7 and 28 days*

Specimen	3 day	7 day	28 day
M	32.4 ± 0.6	36.3 ± 0.5	43.1 ± 0.5
M+CNT	34.9 ± 0.2	40.3 ± 0.7	45.2 ± 0.6
M+MK	34.3 ± 0.8	42.5 ± 0.9	52.2 ± 0.3
M+CNT+MK	33.2 ± 0.8	43.4 ± 0.5	55.2 ± 0.7

4.3. ***Modulus distribution at the ITZ***

The area of interest of 10×10 μm^2 is selected close to the fine aggregate boundary within the ITZ as shown in Figure 11.

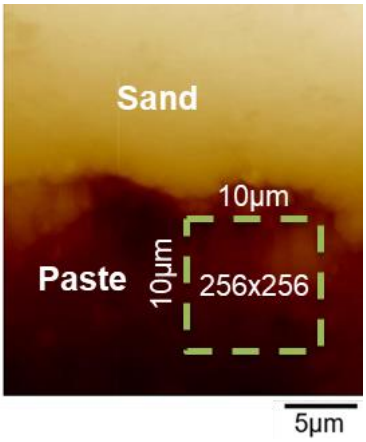

Figure 11: *Test area for AFM-QNM tests on ITZ between sand and cementitious matrix of M+MK sample*

Figure 12 presents the findings of the Young's modulus for the OPC+MK specimen within a 10×10 μm^2 range at the ITZ. To construct the histogram, a total of 65,536 data points were collected and fitted with a probability distribution curve, which can be represented by the following eq. 1:

$$y = \frac{1}{\sigma\sqrt{2\pi}} e^{\left(-\frac{1}{2\sigma^2}(x-\mu)^2\right)} \qquad \text{eq. 1}$$

Where, μ and σ^2 are the mean and variance of the distribution.

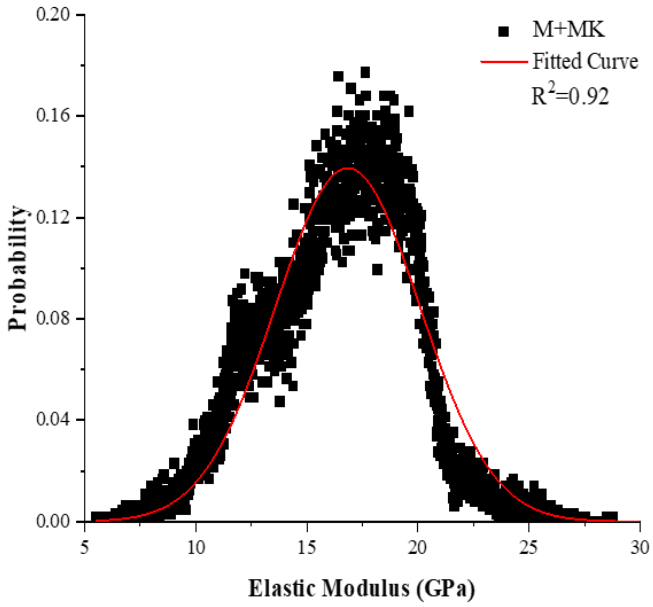

Figure 12: *Probability distribution curve for a 10×10 μm^2 area at the ITZ between sand and cementitious matrix of the M+MK sample*

MOE values within the ITZ of OPC, OPC+CNT and OPC+CNT+MK samples are presented in Figure 13 with the mean modulus reported in Table 7. The modulus of C-S-H is said to be in the range of 8 to 32 GPa [20, 21]. Modulus values higher than 18 GPa are said to correspond to high-density C-S-H. The addition of MK increases the mean modulus and also the area under the curve beyond 18 GPa which implies that the amount of high-density C-S-H is increased. This can be visually understood using the QNM mapping image shown in Figure 14. There is an increase in the region corresponding to high-density C-S-H on addition of MK and nano-reinforcements. In general, using MK as OPC replacement, results in densification of the overall microstructure, including the ITZ, because of the MK's micro-filler effect. This leads in 15 - 20% increases of both the compressive and flexural strength of MK-OPC mortar. The addition of CNTs increases the mean modulus by 22% when compared to plain mortar. The CNT+MK mortar sample presents the highest modulus value at the ITZ. Also, the area under the curve below the 8 GPa gives a qualitative estimate of the porosity of the microstructure. CNTs, with fibrillar morphology and high fracture strain, result in a nanoscale crack arresting mechanism that leads in an increased tensile load bearing capacity; thus, increases of the modulus of ITZ and the flexural strength of nanoreinforced mortars, up to 84%, are observed.

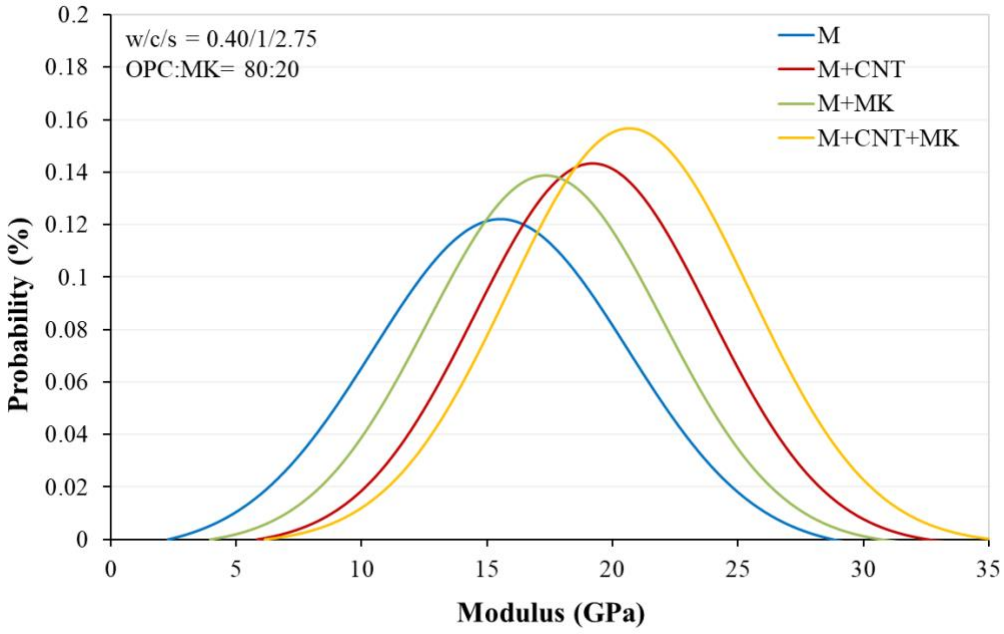

Figure 13: *Probability distribution of Young's modulus for the interface area*

Table 7: Mean modulus at ITZ

Sample	Mean Modulus (GPa)
M	15.2
M+MK	17.4
M+CNT	19.4
M+CNT+MK	21.0

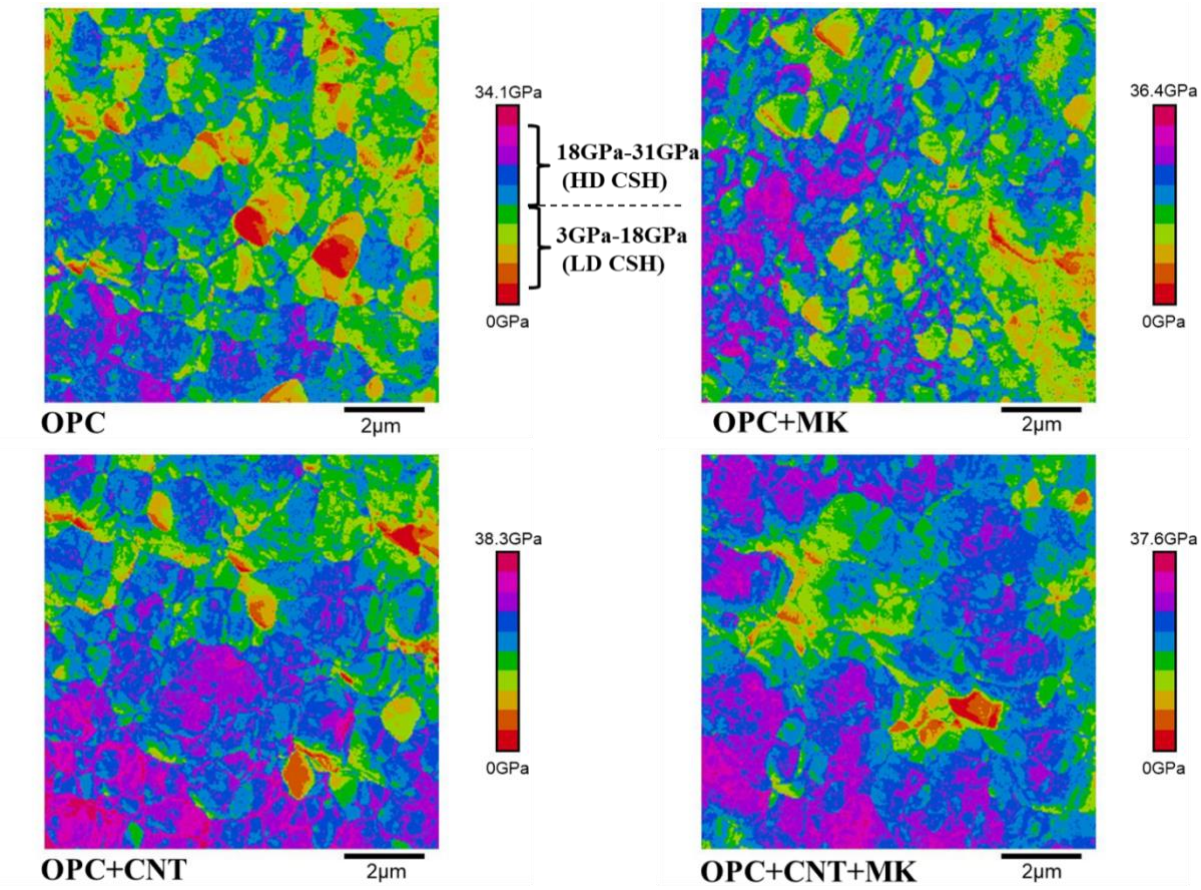

Figure 14: *Elastic modulus contour map at the ITZ*

4.4. ***Chemical characterization of the ITZ***

SEM-EDX analysis is used to determine the chemical composition of the hydration products present at the ITZ. Mapping was performed on multiple lines starting from the fine aggregate (sand) surface towards the matrix as shown in Figure 15.

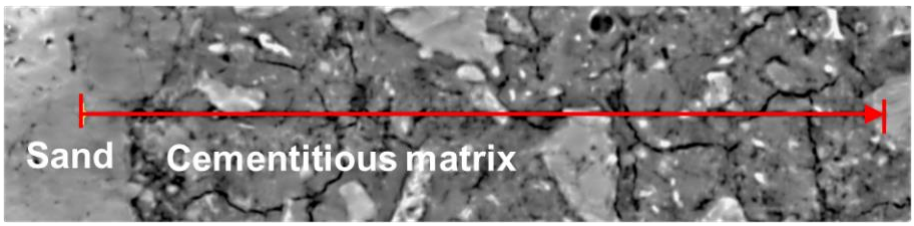

Figure 15: *Line protocol of EDS analysis on an area containing sand and cementitious matrix*

The Ca/Si ratio was taken and developed into a histogram which was fitted using a probability distribution curve presented in Figure 16. The C/S ratio of C-S-H ranges between 1.2 and 2.3 [19]. Values below 2.3 are associated with the polymerization of silicate chain within the C-S-H. Research has shown that a lower Ca/Si ratio at the ITZ indicates a higher amount of C-S-H gel which results in improved strength development [20 – 22]. The addition of MK reduces the amount of $Ca(OH)_2$ by almost 50% due to the pozzolanic reaction which results in the formation of C-S-H and C-A-S-H. The formation of these hydration products decrease the

Ca/Si ratio observed at the ITZ. Additionally, MK contains high amounts of amorphous aluminium which can increase the length of the C-S-H dreierketten chain resulting in the formation of high-density C-S-H that has a lower Ca/Si ratio [23-24]. The addition of CNTs results in an increased amount of high-stiffness C-S-H at the ITZ. This is due to their high surface area which promotes the formation of longer C-S-H dreierketten chain that has a lower Ca/Si ratio and a higher modulus.

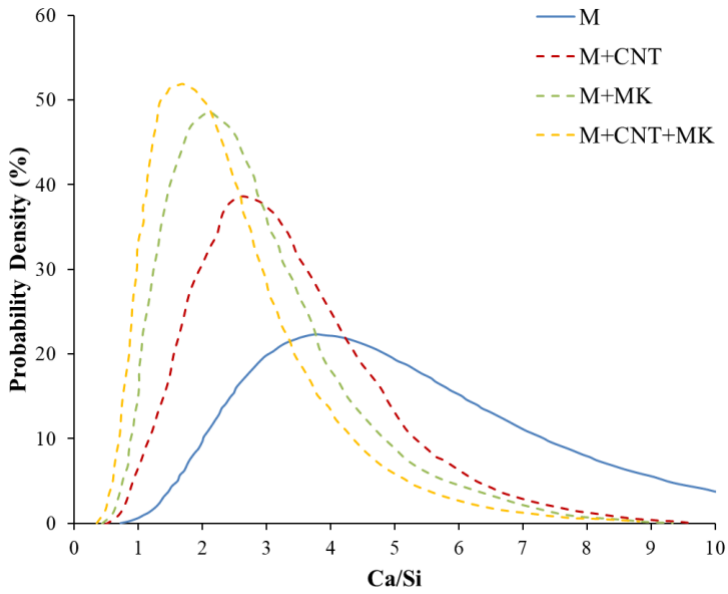

Figure 16: *Ca/Si ratio at the ITZ of sand/cementitious matrix at 28 day*

The results from EDX show that the ITZ has been improved by the addition of both CNT and MK. Figure 17 presents an SEM picture showing the ITZ between CNT modified MK cement paste and fine aggregate at 1 µm resolution.

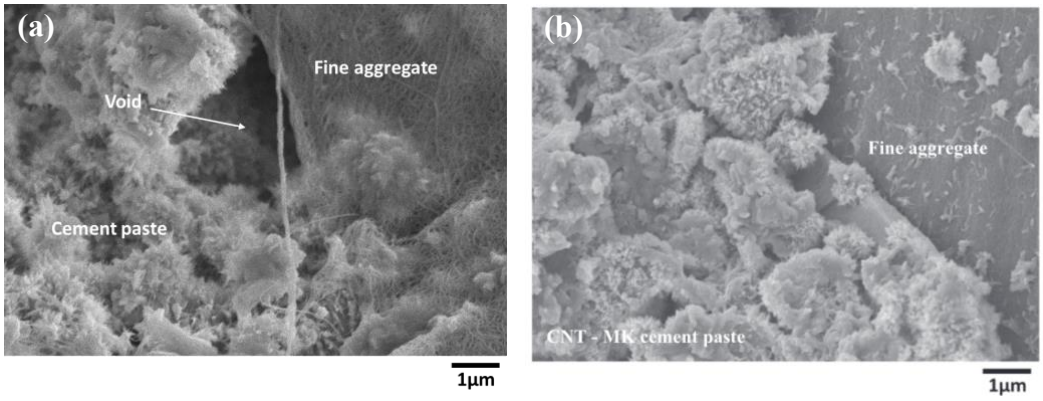

Figure 17: *SEM image of the ITZ between (a) cement paste and fine aggregate (sand) (b)CNT modified MK cement paste and sand*

4.5. **Mechanical Property Results of MK-CNT Concrete**

The modulus of elasticity (MOE) values at 28d mortar and concrete consisting of MK-CNT blends are presented in Figure 18. The CNT incorporation in MK blend results in significant increase in the MOE values by 62.8% when compared to plain concrete. Comparing the

increase in Modulus of Elasticity (MOE) in MK-CNT mortar and MK-CNT concrete to their respective control mixes reveals a higher improvement in MOE for mortar. This is because concrete has 44% fewer CNTs than mortar (3.6×10^{11}).

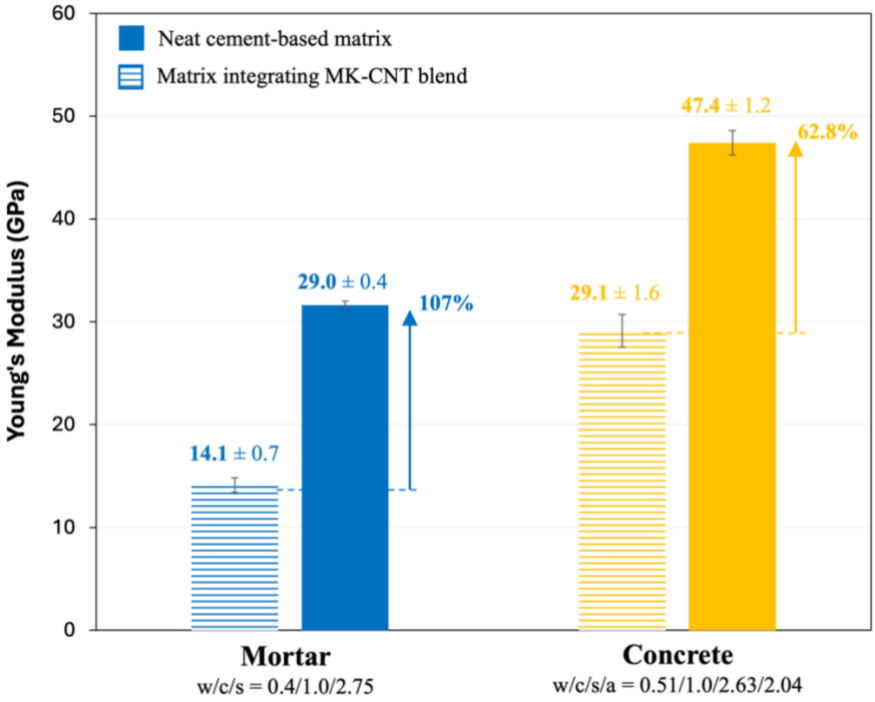

***Figure 18**: Young's modulus of 28d mortar and concrete integrated with MK-CNT blend*

The flexural strength and compressive strength results of 28d MK-concrete reinforced with 0.1 wt% CNTs and CNFs are presented in Table 8. The incorporation of carbon nanotubes (CNTs) into MK-concrete yields a substantial enhancement in flexural strength, with a remarkable 70.3% increase compared to plain concrete. Additionally, the compressive strength exhibits a substantial 42.8% improvement.

***Table 8**: Flexural and Compressive strength of 28d concrete incorporating MK-CNT blend*

Specimen	Fiber count	Flexural Strength (MPa)	Compressive Strength (MPa)
Concrete	-	6.4 ± 1.5	44.6 ± 2.4
Concrete + MK-CNT	2.5×10^{11}	10.9± 1.2	63.7 ± 3.1

5. Conclusions

Typically, MK-based cementitious materials can exhibit negligible tensile strain energy absorption capacity due to their brittle behavior. The experimental study shows that the addition of small amounts of well-dispersed CNTs (0.1 wt%, by mass of binder) in metakaolin-based cementitious composites with 20% replacement can lead to substantial improvements in MOE and post-crack ductility. The pozzolanic reaction of MK densifies the microstructure leading to an improvement in compressive strength by 21% and MOE by 34% compared to OPC mortar. Compared to the MK-Mortar, the CNT reinforced MK-Mortar nanocomposite exhibited 88% increase in flexural strength and 107% increase in MOE. Moreover, the tensile strain energy absorption capacity was improved by 1.8x at the elastic stage. The I_5, I_{10} and I_{20}

toughness indices showed improvements of 45%-110%, which demonstrates the ability of the MK-based cementitious nanocomposite to absorb energy at the post-crack stage. This performance can be related to the proper function of MWCNTs in bridging nano cracks, increasing the ultimate strain capacity and, by extension prolonging the elastic stage and failure of nanoreinforced mortars.

Using Quantitative Nanomechanical Mapping (QNM) technique, significant strengthening of the interfacial transition zone between the sand and cementitious matrix was observed for MK-cement mortar using low concentrations of monodispersed carbon nanotubes (CNT). Nanoscale imaging and property mapping at the ITZ revealed that the local structure/morphology of the interface has improved, resulting in an impressive increase in the modulus of elasticity (+27%). Addition of 0.1 wt% CNTs modified the polymerization of the silicate chain within the C-S-H of the interface between sand and cementitious matrix at the nanoscale level. This helps in explaining the observed increases in the macro-mechanical properties.

The incorporation of CNTs in MK-OPC concrete provides concrete with a toughening mechanism by reinforcing the nanostructure of C-S-H and by modifying the interface between the aggregates and the cementitious matrix. This enhances the concrete's load transfer efficiency at large deformations.

6. References

[1] I. Diaz-Loya, M. Juenger, S. Seraj, R. Minkara, Extending supplementary cementitious material resources: Reclaimed and remediated fly ash and natural pozzolans, Cem. Concr. Compos. 101 (2019) 44–51. https://doi.org/10.1016/j.cemconcomp.2017.06.011.

[2] K. Scrivener, A. Favier, eds., Calcined Clays for Sustainable Concrete: Proceedings of the 1st International Conference on Calcined Clays for Sustainable Concrete, Springer Netherlands, Dordrecht, 2015. https://doi.org/10.1007/978-94-017-9939-3.

[3] J. Han, Z. Shui, G. Wang, J. Shao, Y. Huang, Influence of MK-Based Admixtures on the Early Hydration, Pore Structure and Compressive Strength of Steam Curing Mortars, in: K. Scrivener, A. Favier (Eds.), Calcined Clays Sustain. Concr., Springer Netherlands, Dordrecht, 2015: pp. 219–227. https://doi.org/10.1007/978-94-017-9939-3_27.

[4] B.B. Jindal, T. Alomayri, A. Hasan, C.R. Kaze, Geopolymer concrete with metakaolin for sustainability: a comprehensive review on raw material's properties, synthesis, performance, and potential application, Environ. Sci. Pollut. Res. 30 (2022) 25299–25324. https://doi.org/10.1007/s11356-021-17849-w.

[5] V. Shah, A. Scott, Use of kaolinite clays in development of a low carbon MgO-clay binder system, Cem. Concr. Res. 144 (2021) 106422. https://doi.org/10.1016/j.cemconres.2021.106422.

[6] W. Li, L. Hua, Y. Shi, P. Wang, Z. Liu, D. Cui, X. Sun, Influence of metakaolin on the hydration and microstructure evolution of cement paste during the early stage, Appl. Clay Sci. 229 (2022) 106674. https://doi.org/10.1016/j.clay.2022.106674.

[7] M. Shekarchi, A. Bonakdar, M. Bakhshi, A. Mirdamadi, B. Mobasher, Transport properties in metakaolin blended concrete, Constr. Build. Mater. 24 (2010) 2217–2223. https://doi.org/10.1016/j.conbuildmat.2010.04.035.

[8] A.H. Asbridge, G.A. Chadbourn, C.L. Page, Effects of metakaolin and the interfacial transition zone on the diffusion of chloride ions through cement mortars, Cem. Concr. Res. 31 (2001) 1567–1572. https://doi.org/10.1016/S0008-8846(01)00598-1.

[9] A.M. Mansour, M.I. Al Biajawi, The effect of the addition of metakaolin on the fresh and hardened properties of blended cement products: A review, Mater. Today Proc. 66 (2022) 2811–2817. https://doi.org/10.1016/j.matpr.2022.06.521.

[10] P. Duan, Z. Shui, W. Chen, C. Shen, Effects of metakaolin, silica fume and slag on pore structure, interfacial transition zone and compressive strength of concrete, Constr. Build. Mater. 44 (2013) 1–6. https://doi.org/10.1016/j.conbuildmat.2013.02.075.

[11] M.S. Konsta-Gdoutos, G. Batis, P.A. Danoglidis, A.K. Zacharopoulou, E.K. Zacharopoulou, M.G. Falara, S.P. Shah, Effect of CNT and CNF loading and count on the corrosion resistance, conductivity and mechanical properties of nanomodified OPC mortars, Constr. Build. Mater. 147 (2017) 48–57. https://doi.org/10.1016/j.conbuildmat.2017.04.112.

[12] M.S. Konsta-Gdoutos, P.A. Danoglidis, M.G. Falara, S.F. Nitodas, Fresh and mechanical properties, and strain sensing of nanomodified cement mortars: The effects of MWCNT aspect ratio, density and functionalization, Cem. Concr. Compos. 82 (2017) 137–151. https://doi.org/10.1016/j.cemconcomp.2017.05.004.

[13] E.E. Gdoutos, M.S. Konsta-Gdoutos, P.A. Danoglidis, Portland cement mortar nanocomposites at low carbon nanotube and carbon nanofiber content: A fracture mechanics experimental study, Cem. Concr. Compos. 70 (2016) 110–118. https://doi.org/10.1016/j.cemconcomp.2016.03.010.

[14] P.A. Danoglidis, M.S. Konsta-Gdoutos, E.E. Gdoutos, S.P. Shah, Strength, energy absorption capability and self-sensing properties of multifunctional carbon nanotube reinforced mortars, Constr. Build. Mater. 120 (2016) 265–274. https://doi.org/10.1016/j.conbuildmat.2016.05.049.

[15] E.G. Pinna, D.S. Suarez, G.D. Rosales, M.H. Rodriguez, Hydrometallurgical extraction of Al and Si from kaolinitic clays, REM - Int. Eng. J. 70 (2017) 451–457. https://doi.org/10.1590/0370-44672017700006.
[16] Y. Jenq, S.P. Shah, Two Parameter Fracture Model for Concrete, J. Eng. Mech. 111 (1985) 1227–1241. https://doi.org/10.1061/(ASCE)0733-9399(1985)111:10(1227).
[17] B.V. Derjaguin, V.M. Muller, Yu.P. Toporov, Effect of contact deformations on the adhesion of particles, J. Colloid Interface Sci. 53 (1975) 314–326. https://doi.org/10.1016/0021-9797(75)90018-1.
[18] P.A. Danoglidis, E.E. Gdoutos, M.S. Konsta-Gdoutos, Designing carbon nanotube and nanofiber-polypropylene hybrid cementitious composites with improved pre- and post-crack load carrying and energy absorption capacity, Eng. Fract. Mech. 262 (2022) 108253. https://doi.org/10.1016/j.engfracmech.2022.108253.
[19] S. Wild, J.M. Khatib, Portlandite consumption in metakaolin cement pastes and mortars, Cem. Concr. Res. 27 (1997) 137–146. https://doi.org/10.1016/S0008-8846(96)00187-1.
[20] G. Constantinides, F.-J. Ulm, The nanogranular nature of C–S–H, J. Mech. Phys. Solids 55 (2007) 64–90. https://doi.org/10.1016/j.jmps.2006.06.003.
[21] G. Constantinides, On the use of nanoindentation for cementitious materials, (n.d.) 6.
[22] Y. Gao Northwestern University, Civil and Environmental Engineering, Characterization of Carbon Nanotube Reinforced Cementitious Materials, ProQuest Dissertations & Theses, Ann Arbor, 2018. http://gateway.proquest.com/openurl?url_ver=Z39.88-2004&rft_val_fmt=info:ofi/fmt:kev:mtx:dissertation&res_dat=xri:pqm&rft_dat=xri:pqdiss:10931046 (accessed July 7, 2022).
[23] S. Erdem, A.R. Dawson, N.H. Thom, Influence of the micro- and nanoscale local mechanical properties of the interfacial transition zone on impact behavior of concrete made with different aggregates, Cem. Concr. Res. 42 (2012) 447–458. https://doi.org/10.1016/j.cemconres.2011.11.015.
[24] M.S. Konsta-Gdoutos, Z.S. Metaxa, S.P. Shah, Multi-scale mechanical and fracture characteristics and early-age strain capacity of high performance carbon nanotube/cement nanocomposites, Cem. Concr. Compos. 32 (2010) 110–115. https://doi.org/10.1016/j.cemconcomp.2009.10.007.
[25] P. Mondal, S.P. Shah, L.D. Marks, Nanoscale Characterization of Cementitious Materials, ACI Mater. J. (2008).
[26] D. Zhao, R. Khoshnazar, Microstructure of cement paste incorporating high volume of low-grade metakaolin, Cem. Concr. Compos. 106 (2020) 103453. https://doi.org/10.1016/j.cemconcomp.2019.103453.
[27] Z. Dai, T.T. Tran, J. Skibsted, Aluminum Incorporation in the C-S-H Phase of White Portland Cement-Metakaolin Blends Studied by 27 Al and 29 Si MAS NMR Spectroscopy, J. Am. Ceram. Soc. 97 (2014) 2662–2671. https://doi.org/10.1111/jace.13006.